Tracing the Fate of Atmospheric Nitrate in a Subalpine Watershed Using Δ17 O

Ilann Bourgeois, Joel Savarino, Nicolas Caillon, Hélène Angot, Albane Barbero, Franck Delbart, Didier Voisin, Jean-Christophe Clement

Characterization of Natural and Affected Environments

Tracing the fate of atmospheric nitrate in a subalpine watershed using #O

Ilann Bourgeois, Joël Savarino, Nicolas Caillon, Helene Angot, Albane Barbero, Franck Delbart, Didier Voisin, and Jean-Christophe Clement

Environ. Sci. Technol., **Just Accepted Manuscript** • DOI: 10.1021/acs.est.7b02395 • Publication Date (Web): 19 Apr 2018

Tracing the fate of atmospheric nitrate in a subalpine watershed using $\Delta^{17}O$

Ilann Bourgeois[1,2,], Joel Savarino[1], Nicolas Caillon[1], Hélène Angot[1,a], Albane Barbero[1,b], Franck Delbart[3], Didier Voisin[1], and Jean-Christophe Clément[2,c]*

[1]Univ. Grenoble Alpes, CNRS, IRD, Grenoble INP, Institut des Géosciences de l'Environnement, IGE, 38000, Grenoble, France

[2]Univ. Grenoble Alpes, CNRS, Laboratoire d'Ecologie Alpine, LECA, 38000, Grenoble, France

[3]Univ. Grenoble Alpes, CNRS, Station Alpine Joseph Fourier, SAJF, 38000, Grenoble, France

[a]Now at Institute for Data, Systems and Society, Massachusetts Institute of Technology, Cambridge, MA, USA

[b]Now at Servicio Meteorológico Nacional - Gerencia Investigación, Desarollo y Capacitación, Buenos-Aires, Argentina

[c]Now at Univ. Savoie Mont Blanc, INRA, Centre Alpin de Recherche sur les Réseaux Trophiques des Ecosystèmes Limniques, CARRTEL, 74200, Thonon-Les Bains, France

*ilann.bourgeois@univ-grenoble-alpes.fr

Words count: 5879 (including abstract) / Abstract: 191 words

Figures: 4 (1200 words)

Abstract

Nitrogen is an essential nutrient for life on Earth, but in excess, it can lead to environmental issues (e.g., N saturation, loss of biodiversity, acidification of lakes, etc.). Understanding the nitrogen budget (*i.e.*, inputs and outputs) is essential to evaluate the prospective decay of the ecosystem services (e.g., freshwater quality, erosion control, loss of high patrimonial-value plant species, etc.) that subalpine headwater catchments provide, especially as these ecosystems experience high atmospheric nitrogen deposition. Here, we use a multi-isotopic tracer ($\Delta^{17}O$, $\delta^{15}N$ and $\delta^{18}O$) of nitrate in aerosols, snow and streams to assess the fate of atmospherically deposited nitrate in the subalpine watershed of the Lautaret Pass (French Alps). We show that atmospheric deposition contributes significantly to stream nitrate pool year-round, either by direct inputs (up to 35 %) or by *in situ* nitrification of atmospheric ammonium (up to 35 %). Snowmelt in particular leads to high exports of atmospheric nitrate, most likely fast enough to impede assimilation by surrounding ecosystems. Yet, in a context of climate change, with shorter snow seasons, and increasing nitrogen emissions, our results hint at possibly stronger ecological consequences of nitrogen atmospheric deposition in the close future.

Keywords: atmospheric deposition, nitrate isotopes, subalpine streams, Lautaret Pass

TOC

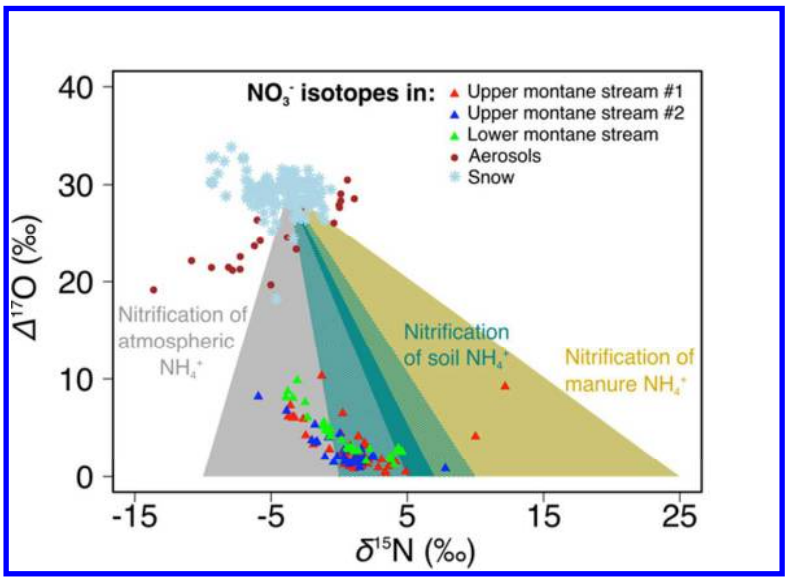

1. Introduction

Reactive Nitrogen (Nr) has long been known for its duality. At low to moderate concentrations, it is an essential nutrient for natural ecosystems in general, and plant nutrition in particular ([1]). In excess, Nr becomes an environmental issue for endemic terrestrial plant species and aquatic ecosystems ([2–4]), and may pose threats to human health ([5]). Human activities have increased N input to the environment by 150% over the last century ([6]), with a rising contribution – among other distribution processes – of atmospheric deposition ([7,8]). Fossil-fuel combustion, agriculture and food production are responsible for direct or indirect emissions of atmospheric N-species with the capacity to reach remote ecosystems such as mountainous regions ([9,10]) where Nr equilibrium is very sensitive to small perturbations ([11,12]). Alpine and subalpine watersheds are particularly vulnerable to this increasing Nr-supply ([13,14]), as they are usually N-limited ecosystems ([15]). The critical load for these ecosystems has been estimated to 1-4 kg-N.ha^{-1}.yr^{-1}, making alpine and subalpine grasslands the most sensitive to N deposition among grasslands and tall forb habitats ([16–18]). In some regions of the globe, such as in the Colorado Front Range, USA, shifts from N-limitation to N-saturation state have been observed leading to regional and national policies to regulate this phenomenon ([19–21]). As a consequence of increasing nitrogen deposition, a slow but persistent change of alpine and subalpine landscape has been noticed in several regions ([22,23]). Species more competitive for nitrogen uptake tend to develop in abundance at the expense of usually oligotrophic native plants, leading to plant diversity loss and changes in ecosystem functioning and services.

Freshwater quality and erosion control are, per instance, threatened by this cascade of changes ([24,25]). Yet, and mainly because of the paucity of monitoring facilities in isolated areas and of the logistical difficulties in accessing these regions, key biogeochemical processes regulating N cycling in mountains are still not well understood ([26]).

More specifically, atmospheric nitrate (NO_3^-) and ammonium (NH_4^+), deriving principally from anthropogenic NO_x (NO and NO_2) and agricultural NH_3 emissions, are transferred to the land surface through wet and dry deposition. Dissolved inorganic nitrogen (DIN) species (*i.e.*, NO_3^- and NH_4^+) are of capital importance in ecological studies given their high solubility in water; the strong hydrological connectivity and typical topography of alpine and subalpine watersheds can lead to a fast transport and a potentially long reach of the above-mentioned nutrients in surrounding ecosystems ([27,28]). Traditionally, environmental studies on NO_3^- sources partitioning are essentially based on $\delta^{15}N$ and $\delta^{18}O$-NO_3^- values ([29–31]), to constrain the biogeochemical processes affecting the various N forms in mountains. Yet, the wide range of observed values for $\delta^{15}N$ and $\delta^{18}O$-NO_3^- from atmospheric and other sources limits accurate quantification of contributing sources ([32,33]).

In this study we focus – for the first time (to the best of our knowledge) – on year-round NO_3^- dynamics in a mountainous watershed in the French Alps, using a multi-isotopic ($\Delta^{17}O$, $\delta^{18}O$, $\delta^{15}N$) tracer of NO_3^- in subalpine surface waters. This relatively new method has been increasingly used, as it enables a more refined understanding of atmospheric NO_3^- ($NO_3^-_{atm}$) contribution to ecosystems N pool ([32,34,35]). With the aim to clearly delineate the fate of atmospheric Nr in a subalpine watershed, we first characterized the triple isotopic composition of NO_3^- in aerosols and snow deposited in high altitude catchments (> 1000m a.s.l.) of the central French Alps (*i.e.*, the input

flux). Second, we evaluated the fate of the deposited $NO_3^-_{atm}$ by monitoring NO_3^- riverine exports from the watersheds (*i.e.*, the output flux).

We hypothesized that (i) the triple isotopes approach will enable a clear delineation of NO_3^- sources and the quantification of their respective contribution to small and medium-scale watersheds N budget and (ii) seasonal dynamics of $NO_3^-_{atm}$ exports in stream will provide additional insights on N cycling controls in high altitude catchments.

2. Material and Methods

2.1 Study Site

The studied catchments are located in the upper Romanche valley, near the Lautaret Pass (central French Alps, SI Figure S1). The experimental site is part of the national research infrastructure for the study of continental ecosystems and their biodiversity (AnaEE – France, https://www.anaee-france.fr), and of the Long Term Ecological Research network (LTER, https://lternet.edu). The streams monitored throughout 2015 are located close to the research facilities of the Alpine Research Station (Station Alpine Joseph Fourier (SAJF), CNRS-UGA, UMS 3370, https://www.jardinalpindulautaret.fr), where atmospheric and climatic parameters were monitored (Figure S2).

The climate is subalpine with a strong continental influence. The annual precipitation in 2015 (year of study) was 537 mm, significantly drier than the mean annual precipitation of 956 mm observed between 2004 and 2013 ([36]). In 2015, *ca.* 45 % of the precipitation occurred during the growing season from snowmelt (in April) to late September. Winters are cold and snowy. The mean temperature was -7.5 °C in

February 2015 and 13.9 °C in July 2015. More detailed information about the sampling site can be found elsewhere ([36,37]).

The first studied sub-watershed (hereafter called Lautaret) is mainly constituted of calcareous substrate and extends over 3.4 km². At the outlet of this sub-watershed runs a stream called Tufiere. Samples were collected at an altitude of *ca.* 2015 m a.s.l, just before the stream merges with the outlet of the second sampled watershed (Figure S1). Altitude on this watershed spans from 1665 to 2725 m a.s.l. Mean slope is 25%, and the vegetation cover Normalized Difference Vegetation Index (NDVI) is 0.38.

The second sub-watershed (hereafter called Laurichard) is constituted of granitic rocks on an ancient volcanic layer and extends over 5.3 km². It is part of the North exposed side of the Combeynot mountain range, which highest peak culminates at 3155 m. The Laurichard stream, fed in part by glacier melt, runs down this mountainous area and is sampled downhill, just before it joins the Tufiere stream. Altitude on this watershed ranges from 1665 to 3155 m a.s.l. Mean slope is 30%, and the vegetation cover NDVI is 0.33.

The last river is Romanche, which integrates the response of the whole Romanche Valley, and is fueled by smaller tributaries such as Tufiere and Laurichard from the Lautaret Pass and the Ecrins National Park down to the artificial Chambon Lake. Our sampling point for this river is about 1000 m lower in altitude and approximately 12 km away from the first two tributaries (contributing area ≈ 220 km²).

2.2 Field sampling

Aerosols were collected on the Lautaret watershed from November 2014 to September 2015 using a homemade apparatus (similar to a Digitel® DA77) equipped

with a Digitel® PM2.5 cutting head. We used QMA Whatman quartz filters for aerosols collection, burnt at 800 °C for 1 h to lower the blank signal ([38]). Filters were changed on a weekly basis, thus accumulating enough material for isotopic analysis. Airflow was fixed at 0.5 m^3 per hour.

From December 2014 to April 2015 a snow pit (SP) was dug every month on the Lautaret watershed to provide profiles of $NO_3^-{}_{atm}$ concentration and isotopic values in the snowpack. For each pit, snow was dug until the soil was reached, then after cleaning the vertical profile, samples were collected every 3 cm starting from surface snow.

Water samples were collected in the three streams (SI Figure S1, in red) from November 2014 to December 2015 to obtain a full one-year hydrological cycle and stream N chemistry. The samples were taken according to the Niwot Ridge LTER protocol ([39]). Samples were taken on a weekly basis when possible, and at most 2 weeks separated two consecutive samples.

More details regarding aerosols, snow and water sampling can be found in the SI, Appendix 1. Unfortunately, neither rivers discharge measurements nor wet deposition collection could be done at the time of the study because of the lack of equipment. Appreciation of snowmelt timeframe, peak and length was based on visual observation of snow cover and rivers flow. The Laurichard stream could not be sampled from mid-January to mid-April as the riverbed was completely covered by the snowpack.

2.3 Samples pre-treatment and NO_3^- concentration analysis

Aerosols samples were analyzed by extracting NO_3^- from filters, immersed in 40 mL of ultrapure water in a centrifugal ultrafiltration unit (Milipore Centricon plus-70, 100

167 000 Daltons), shaken a few times, and then centrifuged at 4500 RPM for 20 minutes.
168 The extract was then collected in a 50 mL Corning® centrifuge tube and kept frozen
169 until further analysis.
170 Water and snow samples underwent the same pre-treatment for isotopic analysis.
171 Frozen samples were melted at room temperature overnight before being filtered
172 using 0.45 µm Whatman GD/X syringe filters linked to a peristaltic pump.
173 Ultimately, aerosols, snow and stream samples were concentrated using an anionic
174 resin (0.6 mL AG 1-X8 resin, Cl^--form, Bio-Rad) with recovery efficiency over 98.5%
175 ([40]) and eluted with 10 mL of a 1 M NaCl solution for isotopic analysis ([41]). Sample
176 aliquots were taken before the resin concentration step for [NO_3^-] determination using
177 a Continuous Flow Analysis spectrophotometer (SEAL Analyzer QuAAtro) based on
178 cadmium-reduction of NO_3^- to nitrite ([42]). [NO_3^-] values are given with an uncertainty
179 of 0.02 mg.L^{-1}, calculated as the mean standard deviation of ten successive
180 measurements of the calibrating standards.
181

182 **2.4 Isotopic analysis**

183 Aerosols, snow and river samples were analyzed for $\Delta^{17}O$, $\delta^{18}O$ and $\delta^{15}N$ of NO_3^-
184 using the bacterial denitrifier technique in combination with the N_2O gold
185 decomposition method ([43–45]). More details about the analytical procedure can be
186 found elsewhere ([46]) and in the SI, Appendix 1.
187 All samples isotopic values were corrected for any isotopic effect possibly occurring
188 during the procedure by processing simultaneously international reference materials
189 (International Atomic Energy Agency USGS 32, USGS 34 and USGS 35) through the
190 same analytical batch. The isotopic standards were prepared in the same
191 background matrix as samples (*i.e.*, 1M NaCl). Standard deviation of the residuals

from the linear regression between the measured reference standards (n = 20) and their expected values served as indicator of the accuracy of the method. In our study, the $\Delta^{17}O$, $\delta^{18}O$ and $\delta^{15}N$ values of aerosols, snow and streams NO_3^- are given, with respect to atmospheric N_2 (AIR) and Vienna Standard Mean Ocean Water (VSMOW) standards, with a mean uncertainty of 0.2, 1.4 and 0.4 ‰ respectively.

2.5 End-member mixing analysis

The triple stable isotope approach using $^{18}O/^{16}O$ and $^{17}O/^{16}O$ enables exclusive quantification of unprocessed $NO_3^-_{atm}$. Because chemical pathways leading to the production of atmospheric NO_3^- involve NO_x oxidation by ozone, which is the bearer of ^{17}O-excess in the first place, it shows a significant positive deviation from the terrestrial fractionation line (TFL: $\delta^{17}O \approx 0.52 * \delta^{18}O$) ([47,48]). $\Delta^{17}O$ is a quantification of this deviation from the TFL, calculated as $\Delta^{17}O = \delta^{17}O - 0.52 * \delta^{18}O$ in the present work. $\Delta^{17}O$ value of atmospheric NO_3^- generally ranges between 20 and 35 ‰ in temperate latitudes ([46,49]) whereas $\Delta^{17}O$ value of NO_3^- from all other sources (industrial fertilizers, nitrification) or biologically processed $NO_3^-_{atm}$, is 0 ([32,50]). In this study, we used these two distinct $\Delta^{17}O$ values as end-members in a simple mixing model to quantify unprocessed $NO_3^-_{atm}$ proportion in streams. Calculation of atmospheric contribution, noted f_{atm}, was derived from the following equation:

(Eq.1) $$\boldsymbol{\Delta^{17}O\text{-}NO_3^-_{sample} = f_{atm} * \Delta^{17}O\text{-}NO_3^-_{atm} + (1- f_{atm}) * \Delta^{17}O\text{-}NO_3^-_{bio}}$$

With $\boldsymbol{f_{atm}}$ (= $\%NO_3^-_{atm}$), the mole fraction of the atmospheric contribution ([32]), $\boldsymbol{\Delta^{17}O\text{-}NO_3^-_{sample}}$ the measured value of $\Delta^{17}O\text{-}NO_3^-$ in a sample and $\boldsymbol{\Delta^{17}O\text{-}NO_3^-_{bio}}$ the value of ^{17}O-excess of biologically-derived NO_3^- ($NO_3^-_{bio}$).

As $\Delta^{17}O\text{-}NO_3^-_{bio}$ = 0 ‰ ([32]), Eq.1 simplifies to

(Eq. 2) $$f_{atm} = (\Delta^{17}O\text{-}NO_3^-_{sample} / \Delta^{17}O\text{-}NO_3^-_{atm}) * 100$$

Choice for the atmospheric end-member values of $\Delta^{17}O\text{-}NO_3^-_{atm}$ is further discussed in section 4.1.

Post-deposition processes such as denitrification or assimilation should enrich $\delta^{18}O$ and $\delta^{15}N$ along a 2:1 to 1:1 line ([51,52]), but co-occurring soil production of NO_3^- by nitrification can lead to lower enrichment proportions ([53]). The $\Delta^{17}O$ value of residual NO_3^- are unaffected by post-deposition processes leading to NO_3^- loss because it is independent of the absolute $\delta^{18}O$ values ([32]). It therefore provides a robust quantification of unprocessed $NO_3^-_{atm}$, and subsequently, of $NO_3^-_{bio}$ as described in Eq. 2.

2.6 Statistical Analysis

We used two non-parametric statistical tests in our study. The choice for non-parametric tests lies in the small population size of the aerosols (n=26), snow (n=30, 22, 29, 36 and 26 for December, January, February, March and April SP, respectively), and stream water samples (n=42, 29 and 28 for Tufiere, Laurichard and Romanche, respectively).

A Mann-Whitney test was applied on river samples to determine whether mean concentrations and isotopic values were significantly different between streams. A Spearman test was applied to evaluate the correlation between stream water parameters (typically $\Delta^{17}O$, $\delta^{18}O$, $\delta^{15}N$ and $[NO_3^-]$). Differences and correlations were held significant when the *p* value reached a 0.01 credible interval.

All statistical analyses were conducted using R software (v3.2.3).

3. Results

3.1 Nitrate input to ecosystems: $NO_3^-{}_{atm}$

Evolution of mean concentration, $\Delta^{17}O$, $\delta^{18}O$ and $\delta^{15}N$ of NO_3^- in snow pits throughout the winter and in aerosols throughout year 2015 can be found in Table 1 and Figure S3. First snow falls occurred mid-November 2014 with several freeze-thaw events before it started to accumulate. On days of snow pits sample collection, snowpack depths were 66, 64, 139, 142 and 101 cm in December 2014, January, February, March and April 2015, respectively. Maximum snow accumulation (*ca.* 1.6 m) occurred early March 2015 (SI, Appendix 1). By the end of April 2015, the snowpack had completely melted. In December and January, low [NO_3^-] were measured in all snow pits layers (SI, Figure S3a). In February and March, a peak of [NO_3^-] up to 5 mg.L^{-1} between 70 and 90 cm of snow accumulation was recorded. This peak was also measured in April (orange line in Figure S3), but at a lower depth (40-60 cm) and to a lesser extent (2.7 mg.L^{-1}), due to elution of the snowpack NO_3^- by snowmelt water. $\Delta^{17}O$-NO_3^- in snow varied between 20 and 35 ‰ (SI, Figure S3b), well within the atmospheric range of NO_3^- isotopic values reported in the literature ([46,54]). $\delta^{18}O$ and $\delta^{15}N$ values were between 60 and 90 ‰ and -10 and 0 ‰, respectively (SI, Figure S3c and d), consistent with a reservoir exclusively made of $NO_3^-{}_{atm}$ ([51]). Mean (± standard deviation) isotopic values of snow NO_3^- were 29.3 ± 1.6, 77.0 ± 5.6 and -3.6 ± 1.6 ‰ for $\Delta^{17}O$, $\delta^{18}O$ and $\delta^{15}N$, respectively. Mean isotopic values of NO_3^- in aerosols were also consistent with other measurements of particulate NO_3^- ([55]), featuring significantly lower mean $\Delta^{17}O$-NO_3^-

and δ^{15}N-NO_3^- in summer (23.1 ± 2.4 and -6.5 ± 3.4 ‰, respectively) than in winter (28.9 ± 1.7 and -1.0 ± 1.7 ‰, respectively), a temporal pattern discussed in the SI, Appendix 3. Winter aerosols NO_3^- isotopic values were in the range of the snowpack NO_3^- values.

3.2 Nitrate output in rivers

All streams [NO_3^-] data can be found in the SI, Table S1. Laurichard showed significantly higher year-round [NO_3^-] compared to the other streams, with a mean value of 2.6 ± 1.3 mg.L^{-1}. Mean annual [NO_3^-] was 0.09 ± 0.06 mg.L^{-1} and 1.02 ± 0.48 mg.L^{-1} in Tufiere and Romanche, respectively. Seasonal variations were similar in all streams, featuring higher [NO_3^-] in late spring and lower [NO_3^-] in summer (Figure 1a).

Tufiere had the widest range in Δ^{17}O-NO_3^- values, varying from 0.5 to 10.3 ‰, with a mean value of 3.2 ± 2.4 ‰. Δ^{17}O-NO_3^- values in Laurichard ranged from 0.8 to 8.2 ‰, with a mean value of 2.8 ± 1.7 ‰. In Romanche, Δ^{17}O-NO_3^- values remained above 3 ‰ for a period spanning several months, with a mean value of 4.3 ± 2.3 ‰ (Figure 1b). Mean Δ^{17}O-NO_3^- was significantly higher in Romanche than in Tufiere and Laurichard, whereas there was no significant difference between Tufiere and Laurichard mean Δ^{17}O-NO_3^- (p-value = 0.5).

All streams showed similar range for δ^{18}O-NO_3^- and δ^{15}N-NO_3^-, between -5 and 25 ‰ for δ^{18}O-NO_3^- and between -6 and 13 ‰ for δ^{15}N-NO_3^-. Our findings were in the same range of previously measured NO_3^- isotopic values in alpine streams ([31,56,57]).

4. Discussion

4.1 $NO_3^-_{atm}$ end-member

Our choice to use snow-NO_3^- as the atmospheric end-member laid on simple but robust assumptions. First, snow is a good conservator of atmospheric nitrate in high accumulation sites (> 30 cm of snow accumulation) and preserves its isotopic composition ([49,59]). Second, the snowpack is representative of winter bulk deposition, as it aggregates both wet and dry deposition ([60,61]). Third, most of $NO_3^-_{atm}$ measured in streams was assumed to come from snowmelt, as previously observed in other seasonally snow-covered catchments ([60,62]). Little temporal variation of NO_3^- concentration and isotopic values in snow pits profiles, along with no isotopic evidence of post-deposition processes further supported this assumption (SI, Appendix 2, Figures S3 and S4).

By inputting mean snow $\Delta^{17}O\text{-}NO_3^-$ in Eq.2, we obtained:

(Eq.3) $$f_{atm} = (\Delta^{17}O\text{-}NO_3^-_{sample} / 29.3) * 100$$

The error range on f_{atm} was inferred from snow $\Delta^{17}O\text{-}NO_3^-$ standard deviation, and calculated as 2 %.

It must be underlined that snow as atmospheric end-member might not account correctly for wet or dry deposition of NO_3^- in summer. Wet N deposition has *de facto* been shown to contribute significantly to freshwaters NO_3- contents, either through direct inputs due to flashy hydrology ([34,56]) or through indirect contribution *via* enhanced nitrification of atmospheric NH_4^+ ([63]). We show that summer deposition of NO_3^- (wet or dry) as atmospheric end-member results in higher calculated $NO_3^-_{atm}$ fraction in streams, up to 6% in this study (SI, Appendix 3). For that reason, all calculated f_{atm} values in the following sections must be considered as a lower estimate of $NO_3^-_{atm}$ inputs in this system.

317

318 **4.2 Identification of $NO_3^-_{bio}$ sources**

319 No correlation was found between $\Delta^{17}O\text{-}NO_3^-$ and $[NO_3^-]$ in Tufiere, Laurichard and
320 Romanche (Figure 2a, b and c), indicating that $NO_3^-_{atm}$ is not the main contributor to
321 streams nitrate load on a yearly basis. For all streams, $\Delta^{17}O\text{-}NO_3^-$ was significantly
322 correlated to $\delta^{18}O\text{-}NO_3^-$ (Figure 2d, e and f) with the best correlation found in
323 Romanche. Deviations from linear regressions are attributed to occasionally intense
324 biological processes affecting $\delta^{18}O$ signal but leaving $\Delta^{17}O$ intact. Otherwise, the
325 strong linear correlations observed here suggest that mixing of sources more than
326 biological processes could explain the observed seasonal variations of NO_3^- isotopic
327 values. As a consequence, by extrapolating this linear relationship to $\Delta^{17}O\text{-}NO_3^- = 0$
328 (*i.e.*, 100 % biologically derived NO_3^-), we can determine the mean $\delta^{18}O$ value of
329 $NO_3^-_{bio}$ produced in the three watersheds: -6.0, -4.6 and -6.6 ‰ in Tufiere, Laurichard
330 and Romanche, respectively. These results for $NO_3^-_{bio}$ were consistent with other
331 studies estimation of $\delta^{18}O\text{-}NO_3^-_{bio}$ in streams, either calculated *via* the same method
332 ([32,64]) or deduced from measured $\delta^{18}O$ values of soil-water and O_2, assuming they
333 respectively contributed to NO_3^--O accordingly to $\delta^{18}O\text{-}NO_3^- = 1/3\ (\delta^{18}O\text{-}O_2) + 2/3$
334 $(\delta^{18}O\text{-}H_2O)$ ([51,58]). Note that our approach (*i.e.*, $\Delta^{17}O$ *vs* $\delta^{18}O$) might yield lower
335 uncertainty compared to the traditional one (*i.e.*, $\delta^{18}O$ calculation) which comes with
336 a number of assumptions and caveats that are thoroughly dissected elsewhere ([58,65]).
337 Conversely, we found a significant negative correlation between $\Delta^{17}O\text{-}NO_3^-$ and $\delta^{15}N\text{-}$
338 NO_3^- (Figure 2g, h and i) in the three streams, with once again the best fit for
339 Romanche. With the same method as cited above, we can infer the mean $\delta^{15}N\text{-}NO_3^-$
340 $_{bio}$: 4.4, 5.0 and 6.1 ‰ in Tufiere, Laurichard and Romanche, respectively. These
341 values characterizing the $NO_3^-_{bio}$ end-member are typical of NO_3^- produced from soil

NH_4^+ nitrification ([51]). On the other hand, extrapolating this correlation to $\Delta^{17}O\text{-}NO_3^-$ = 29.3 ‰ (*i.e.*, 100% $NO_3^-_{atm}$) should give $\delta^{15}N\text{-}NO_3^-_{atm}$ and $\delta^{18}O\text{-}NO_3^-_{atm}$ consistent with otherwise measured snow NO_3^- isotopic values. We found values of 77.7, 79.0 and 74.7 ‰ for $\delta^{18}O\text{-}NO_3^-_{atm}$ in Tufiere, Laurichard and Romanche, respectively, consistent with the mean $\delta^{18}O$ value of 77.0 ‰ measured for snow NO_3^- (Table 1). Surprisingly, $\delta^{15}N\text{-}NO_3^-_{atm}$ values of *ca.* -30 ‰ were inferred in all streams, far from measured $\delta^{15}N\text{-}NO_3^-$ in snow and aerosols (Table 1) and from existing literature data showing a range of $\delta^{15}N$ values for NO_3^- between -15 and 15 ‰ ([51,66–68]). This suggested that a two end-members mixing model cannot account for the different sources of N that might have served as substrate for nitrification in subalpine meadows, and the subsequent large distribution of $\delta^{15}N\text{-}NO_3^-_{bio}$. Such pattern can only be explained by an additional source of $NO_3^-_{bio}$, with low $\delta^{15}N$ values, leading to the observed weak slopes in Figures 2g, h and i. By lowering the slopes of the correlations, this additional source was responsible for the low extrapolated $\delta^{15}N\text{-}NO_3^-$ values, which in this case (*i.e.*, three sources) do not correspond to any source end-member.

Similar work in alpine watersheds in the Colorado Front Range suggested that possible sources of NO_3^- in streams, apart from snow $NO_3^-_{atm}$, could be nitrification of snow NH_4^+ in the snowpack and in soils during snowmelt, or flushing of soil NO_3^- produced under the snowpack during winter ([29]). Nitrification in the snowpack is highly unlikely; indeed, such a process would have overprinted snow $\Delta^{17}O\text{-}NO_3^-$ values, which is not the case here (SI, Figure S3 and Appendix 2). However, the dual isotopes plot presented in Figure 3 hints at a stronger contribution of atmospheric N deposition – either as snow or rain – than previously assessed in subalpine watersheds. Deposition of $NH_4^+_{atm}$ in particular was likely to enrich soils N pool, and

could account for part of $NO_3^-_{bio}$ exported in streams. Snow at the Lautaret Pass has been shown to hold a non-negligible pool of NH_4^+ – equivalent to NO_3^- pool ([37]) – whereas undetectable [NH_4^+] was monitored in all streams (data not shown) suggesting that NH_4^+ released from snow is either adsorbed on clay minerals or biologically processed. If the entire snow-NH_4^+ pool (if considered about roughly the same size as snow-NO_3^- pool) was nitrified in soils and exported as NO_3^- into streams during snowmelt, it would account for as much as 54 and 18 % of $NO_3^-_{bio}$ production in Tufiere and Laurichard, respectively (Figure 1b). The additional $NO_3^-_{bio}$ exported in streams can only be explained by soil leaching at snowmelt. Strong microbial activity under the snowpack is not uncommon in cold mountainous regions ([36,62,69,70]) and could justify the observed pattern. At snowmelt, cold adapted microbial communities massively turn over when confronted to warmer air temperatures ([71]), releasing nitrified N from lysed cells into the soils where it leaches towards groundwater and streams ([72]). Sources of nitrified N under the snowpack may be related to soil organic matter and litter decomposition ([73]) or soil NH_4^+ pool resulting from previous year's N deposits ([29,72]). At this point we cannot conclude which source contributed the most to $NO_3^-_{bio}$ yield, but overwinter isotopic monitoring of N pools under the snowpack might bring clarification.

4.3 Seasonal variations of $NO_3^-_{atm}$ exports

All stream water samples in this study had positive Δ^{17}O-NO_3^- values, showing unquestionable inputs of $NO_3^-_{atm}$ in all streams year-round (Figure 1b). However, Tufiere and Laurichard, although sampled at the same altitude, showed different NO_3^- export patterns, certainly due to different hydrological behaviors and respective basins characteristics ([58]).

392 NO_3^- dynamic in Tufiere were most likely governed by snowmelt. Brief but high peaks
393 of ^{17}O-excess of NO_3^- in March 2015, coincident with higher [NO_3^-], were attributed to
394 direct runoff of snowmelt water to the stream ([56,64]). Rapid melting of the lower
395 watershed snowpack washed away labile $NO_3^-_{atm}$ deposits and contributed up to 35
396 % of the total stream NO_3^- pool. Leached $NO_3^-_{bio}$ from snow-free soils by subsurface
397 melt or rain water accounted for both higher [NO_3^-] and lower $\Delta^{17}O$-NO_3^- in the
398 stream later in spring ([74]). Gentle hillslopes and the calcareous substrate of the
399 Lautaret sub-watershed were also likely to facilitate snowmelt water infiltration and
400 mixing with groundwater, a common feature in subalpine catchments ([75]). Starting
401 early May, a slow but persistent increase in $\Delta^{17}O$-NO_3^- suggested a resurgence of
402 $NO_3^-_{atm}$ loaded water entering the stream, increasing $NO_3^-_{atm}$ proportion up to 25 %
403 again at the end of August. Significantly higher precipitation in May and in August,
404 compared to the previous months (SI, Figure S2a) could have triggered this
405 resurgence by filling the aquifer with rain water, thus flushing stored water. The wide
406 temporal range of this $\Delta^{17}O$ increase, encompassing six months from May to
407 October, is in line with a temporally spread transit time of infiltrated melt water along
408 an altitude gradient. Direct contribution of rain $NO_3^-_{atm}$ was unlikely to explain such
409 pattern, given the low response of Tufiere [NO_3^-] and $\Delta^{17}O$-NO_3^- to the storm in June
410 (Figure 1a and b). Considering the basin topography and geology (*i.e.*, gentler slopes
411 and higher vegetation cover), most rain N inputs were certainly retained in soils or
412 assimilated before either infiltration or direct runoff of rainwater in Tufiere ([63]).
413 Oppositely, $NO_3^-_{atm}$ contributed only between 4 and 15 % of total NO_3^- in Laurichard
414 stream from April to May (Figure 1b), coincident with the snowmelt period for this
415 northern exposed watershed. Laurichard rock glacier is an actively monitored

permafrost-related landform, which increased surface velocities over the past twenty years hint at increased permafrost temperatures, possibly to the point of thawing ([76]). Considerably higher year-round [NO_3^-] in Laurichard compared to snow-fed Tufiere – by 1-2 orders of magnitude – suggested that Laurichard NO_3^- exports were mainly driven by increasing soil exposure ([77]) more than any other geomorphic or biogeographic feature ([78]). Sources of such elevated levels of NO_3^-, while still debated ([79,80]), were likely linked to glaciers retreat and permafrost thawing leading to enhanced stream solutes fluxes ([81,82]), increased nitrification and/or mobilization of stored N from disturbed soils ([83]). Steeper slopes (SI, Figure S1), and potentially increased deposition loading because of increased orographic precipitations ([21]) – relative to the Lautaret watershed – were certainly responsible for the occasional higher $\Delta^{17}O\text{-}NO_3^-$ peaks, concomitant with rain events (Figure 1b). Lower vegetation cover – and therefore reduced plant $NO_3^-_{atm}$ uptake– and the poor buffering capacity of Laurichard watershed granitic bedrock are additional factors that could have fostered punctually enhanced exports of $NO_3^-_{atm}$ from wet deposition ([77,58]). The storm in June 2015 (Figure S2) led to the strongest input of $NO_3^-_{atm}$ in this stream, accounting for 29 % of Laurichard NO_3^- pool (Figure 1b). Simultaneous $\Delta^{17}O\text{-}NO_3^-$ peaks and [NO_3^-] minima in July and September were further evidence of this flashy hydrology and illustrated stream glacial melt water dilution by rain.

Conversely, we did not observe an early snowmelt runoff-linked peak in Romanche stream water $\Delta^{17}O\text{-}NO_3^-$ in spring. Instead, $NO_3^-_{atm}$ contribution increased steadily from April to July (34 % of $NO_3^-_{atm}$ on July 9th) then declined until reaching a baseflow value of about 5 % of $NO_3^-_{atm}$ during the dormant season. Romanche is the main stream of the valley, fueled by myriad smaller tributaries like Tufiere and Laurichard. Lower altitude catchments contributed most in spring, but as air temperature and

441 solar radiation increased in summer, melting snowpack from higher watersheds of
442 the Ecrins National Park may have led to enhanced $NO_3^-{}_{atm}$ export in Romanche
443 stream leading to the wide $\Delta^{17}O\text{-}NO_3^-$ temporal pattern observed in this stream.
444 Why [NO_3^-] decreased from Laurichard to Romanche is uncertain, but dilution by
445 snow-fed streams like Tufiere between sampling locations is a possibility. Other
446 possible sinks include denitrification, in-stream algal and phytoplankton assimilation
447 or uptake by the riparian vegetation ([85]). Denitrification and assimilation should
448 discriminate $\delta^{18}O$ against $\delta^{15}N$ of residual NO_3^- following a line with a positive slope
449 (*i.e.*, enrich the residual nitrate with heavier isotopes), which was not observed in our
450 study (SI, Figure S5). However, frequent recharge of NO_3^- by smaller tributaries such
451 as Laurichard may have overprinted any biological isotopic signature ([53]).
452 On all basins, the strong controls seemingly exerted either by snowmelt (Tufiere and
453 Romanche) or by glacier melt water (Laurichard) on stream $NO_3^-{}_{atm}$ exports
454 precluded the quantification of the direct $NO_3^-{}_{atm}$ summer deposition contribution.
455 Summer deposition loads of $NO_3^-{}_{atm}$ to streams were either buffered by vegetation
456 uptake and/or soil immobilization on Lautaret watershed, subdued by high $NO_3^-{}_{bio}$
457 except on intense rain events on Laurichard watershed, or combined with the wide
458 temporal response of the Romanche to snowmelt from uplands. Nevertheless,
459 summer deposition of $NH_4^+{}_{atm}$ contributed significantly to subalpine soils N pool and
460 was partly responsible for the $NO_3^-{}_{bio}$ exports in streams.
461 Simultaneous monitoring of $\Delta^{17}O\text{-}NO_3^-$, streams discharge, water isotopes and
462 chemical tracers of hydrological paths remain needed to further constrain water
463 sources and their respective contribution to NO_3^- exports in subalpine streams.
464 Longer monitoring of streams exports is also warranted to better evaluate annual
465 variability in this subalpine watershed, as year 2015 was significantly drier than

previous years at the Lautaret Pass. Hydrological responses to rain events, and resulting NO_3^- export dynamics under different precipitation conditions, need to be assessed.

4.4 Nitrogen saturation and ecological implication

Despite presenting different N export dynamics, all streams shared uninterrupted presence of NO_3^- year-round, with a significant contribution from atmospheric deposition. In a supposedly N-limited ecosystem, such a pattern was unexpected as demand for dissolved inorganic nitrogen (DIN) from plants and microbial communities in spring and summer should have exceeded mobile NO_3^- reservoir in soils, precluding leaching to the streams.

Nitrogen saturation has first been evaluated in an ecosystem subjected to increasing N deposition ([2]). Several stages of saturation have been distinguished, ranging from 0 (N-limited ecosystem) to 3 (fully saturated ecosystem characterized by N-leaching and higher streams $[NO_3^-]$). $[NO_3^-]$ in Tufiere and Romanche was within the range of reported alpine and mountain stream $[NO_3^-]$ ([84]), but $[NO_3^-]$ in Laurichard was higher than in streams pinned as indicators of stage 2 or 3 ([34]). However, similar seasonal variations of $[NO_3^-]$ in Tufiere, Laurichard and Romanche – high in spring after snowmelt, decreasing in summer, then increasing again as air temperature starts falling down (Figure 1) – were symptomatic of plants and microbial biomasses working as N sinks during the growing season. Evaluation of N saturation according to the conceptual model of biological demand exceeded by N supply does not take into account other drivers of N exports ([58]), and may not be adapted to describe the N saturation state of subalpine watersheds. Another approach to N saturation has been described as kinetic N saturation, where the rate of N inputs exceeds the rate of N

assimilation in an ecosystem and its remediation capacity, and can lead to intensive exports of N in streams ([86]). Given the highest percentage of unprocessed $NO_3^-{}_{atm}$ during hydrological events, our results provided additional evidence that catchment hydrology is certainly responsible for the kinetic N saturation in subalpine watersheds. Anyhow, assessment of N deposition load could help us estimate whether the critical threshold has been crossed, as evidenced in other alpine environments ([17,18,87]), and will be the object of future studies.

N inputs at the watershed scale, through $NO_3^-{}_{atm}$ direct contribution or $NH_4^+{}_{atm}$ nitrification, are likely to substantially impact surrounding ecosystems, especially during the growing season following snowmelt. For instance, the lake Chambon, a freshwater reservoir fueled by the Romanche stream, which supplies downhill villages and cities – including Grenoble (163 000 inhabitants) – with drinking water, showed high $NO_3^-{}_{atm}$ contribution from May to November (up to 25 %, Table S2). While $[NO_3^-]$ in the lake averaged 2.0 ± 0.8 $mg.L^{-1}$ during the growing season, far below the limit of 50 $mg.L^{-1}$ (guideline value from The World Health Organization translated in the EU Water Framework Directive 2000/60/EC), the presence of $NO_3^-{}_{atm}$ in this elevated freshwater reservoir is yet another warning signal of potential threats due to atmospherically deposited pollutants. Evidence of lakes fertilization by atmospheric deposition in high altitude watersheds has been demonstrated before ([88]). Fast cycling dynamics of high atmospheric Nr in lakes ([89]) can lead to well-documented ecological consequences such as acidification ([17]), shift of algal and phytoplankton communities ([90,91]) and disturbance of lakes food web ([92]), and highlight the necessity to protect critical water resources. In winter, limited hydrological connectivity between soils and streams cannot explain the year-round export presence of unprocessed $NO_3^-{}_{atm}$ in subalpine streams, highlighting the

potential contribution of groundwater contamination to streams exports. Previous studies also showed that most alpine and subalpine plants acquire N during snowmelt ([93]). In traditionally N-poor subalpine ecosystems, increasing inputs of $NO_3^-{}_{atm}$ together with climate change could accelerate diversity and composition losses of plant communities.

In a 21st century with a shorter snow season, a higher fraction of the yearly deposited NO_3^- will be brought to subalpine ecosystems at a slower rate, during the growth season, instead of abruptly at snowmelt. If NO_3^- saturation is indeed kinetic – as our study suggested – then this climate driven change in NO_3^- influx timing could result in higher NO_3^- absorption in the environment, and lead to capacity saturation. This would come with a wide number of changes in the ecosystem, which have been extensively detailed elsewhere at a global scale ([2,3,8]), and more specifically in high altitude catchments ([11,18,92]).

These findings emphasize the need for more joint monitoring of subalpine soils and plant communities, with the objective being a better understanding of atmospheric N deposition consequences on biogeochemical cycling in these semi-isolated ecosystems. In particular, prospective studies should continue focusing on potential synergetic effects of land use management coupled with atmospheric deposition on ecosystems alteration, to better orient policy makers in N emissions mitigation and adaptation efforts.

Acknowledgments

This study was supported by grants from the Labex OSUG@2020 (“Investissements d’avenir” - ANR10 LABX56), the ARC - Environnement Région Rhone-Alpes and the

Grenoble-Chambéry DIPEE CNRS. This work also benefited from the National Research Agency support ("Investissements d'avenir" - ANR11 INBS-0001AnaEE-Services) and from the SAJF research station (UMR 3370, UGA/CNRS) infrastructures and competences. The study took place on the long-term ecological research site Zone Atelier Alpes, a member of the ILTER-Europe. We would like to thank J.-L. Jaffrezo, F. Masson, V. Lucaire, E. Vince, C. Arnoldi and S. Albertin for help with either laboratory or field work. We acknowledge J. Renaud for help with SIG.

Supporting Information

Appendix 1 includes complementary information on sampling and analytic protocols. Appendix 2 and 3 provide explanation on the choice of snow nitrate as atmospheric end-member. Figures show the study site (S1), the meteorological conditions at the Lautaret Pass in 2015 (S2), the concentration and isotopic values of NO_3^- in snow during winter 2014-2015 (S3), correlation plots of snow NO_3^- isotopic values (S4) and a correlation plot of rivers $\delta^{18}O$ *vs* $\delta^{15}N\text{-}NO_3^-$ (S5). Tables give $[NO_3^-]$ for each sampling date in Tufiere, Laurichard and Romanche (S1) and in the Chambon Lake (S2). This information is available free of charge via the Internet at http://pubs.acs.org.

References

(1) Epstein, E.; Bloom, A. *Mineral Nutrition of Plants Principles and Perspectives, 2nd Edition.*; John Wiley & Sons, 2016.

(2) Aber, J. D.; Nadelhoffer, K. J.; Steudler, P.; Melillo, J. M. Nitrogen Saturation in Northern Forest Ecosystems. *BioScience* **1989**, *39* (6), 378–386.

(3) Vitousek, P. M.; Aber, J. D.; Howarth, R. W.; Likens, G. E.; Matson, P. A.; Schindler, D. W.; Schlesinger, W. H.; Tilman, D. G. HUMAN ALTERATION OF THE GLOBAL NITROGEN CYCLE: SOURCES AND CONSEQUENCES. *Ecol. Appl.* **1997**, *7* (3), 737–750.

(4) Galloway, J. N.; Aber, J. D.; Erisman, J. W.; Seitzinger, S. P.; Howarth, R. W.; Cowling, E. B.; Cosby, B. J. The Nitrogen Cascade. *BioScience* **2003**, *53* (4), 341.

(5) Ward, M. H.; deKok, T. M.; Levallois, P.; Brender, J.; Gulis, G.; Nolan, B. T.; VanDerslice, J. Workgroup Report: Drinking-Water Nitrate and Health—Recent Findings and Research Needs. *Environ. Health Perspect.* **2005**, *113* (11), 1607–1614.

(6) Galloway, J. N.; Dentener, F. J.; Capone, D. G.; Boyer, E. W.; Howarth, R. W.; Seitzinger, S. P.; Asner, G. P.; Cleveland, C. C.; Green, P. A.; Holland, E. A.; et al. Nitrogen Cycles: Past, Present, and Future. *Biogeochemistry* **2004**, *70* (2), 153–226.

(7) Matson, P.; Lohse, K. A.; Hall, S. J. The Globalization of Nitrogen Deposition: Consequences for Terrestrial Ecosystems. *AMBIO J. Hum. Environ.* **2002**, *31* (2), 113.

(8) Galloway, J. N.; Townsend, A. R.; Erisman, J. W.; Bekunda, M.; Cai, Z.; Freney, J. R.; Martinelli, L. A.; Seitzinger, S. P.; Sutton, M. A. Transformation of the nitrogen cycle: recent trends, questions, and potential solutions. *Science* **2008**, *320* (5878), 889–892.

(9) Baron, J. S.; Nydick, K. R.; Rueth, H. M.; Lafrançois, B. M.; Wolfe, A. P. High Elevation Ecosystem Responses to Atmospheric Deposition of Nitrogen in the Colorado Rocky Mountains, USA. In *Global Change and Mountain Regions*; Huber, U. M., Bugmann, H. K. M., Reasoner, M. A., Eds.; Beniston, M., Series Ed.; Springer Netherlands: Dordrecht, 2005; Vol. 23, pp 429–436.

(10) Preunkert, S. A seasonally resolved alpine ice core record of nitrate: Comparison with anthropogenic inventories and estimation of preindustrial emissions of NO in Europe. *J. Geophys. Res.* **2003**, *108* (D21).

(11) Baron, J. S.; Rueth, H. M.; Wolfe, A. M.; Nydick, K. R.; Allstott, E. J.; Minear, J. T.; Moraska, B. Ecosystem Responses to Nitrogen Deposition in the Colorado Front Range.

Ecosystems **2000**, *3* (4), 352–368.
(12) Kirchner, M.; Fegg, W.; Römmelt, H.; Leuchner, M.; Ries, L.; Zimmermann, R.; Michalke, B.; Wallasch, M.; Maguhn, J.; Faus-Kessler, T.; et al. Nitrogen deposition along differently exposed slopes in the Bavarian Alps. *Sci. Total Environ.* **2014**, *470–471*, 895–906.
(13) Clark, C. M.; Morefield, P. E.; Gilliam, F. S.; Pardo, L. H. Estimated losses of plant biodiversity in the United States from historical N deposition (1985–2010). *Ecology* **2013**, *94* (7), 1441–1448.
(14) Burns, D. A. The effects of atmospheric nitrogen deposition in the Rocky Mountains of Colorado and southern Wyoming, USA—a critical review. *Environ. Pollut.* **2004**, *127* (2), 257–269.
(15) Kaye, J. P.; Hart, S. C. Competition for nitrogen between plants and soil microorganisms. *Trends Ecol. Evol.* **1997**, *12* (4), 139–143.
(16) Bobbink, R.; Hettelingh, J.-P.; Review and revision of empirical critical loads and dose-response relationships. *Review and revision of empirical critical loads and dose-response relationships: proceedings of an expert workshop, Noordwijkerhout, 23-25 June 2010*; RIVM: Bilthoven, 2011.
(17) Baron, J. S.; Driscoll, C. T.; Stoddard, J. L.; Richer, E. E. Empirical Critical Loads of Atmospheric Nitrogen Deposition for Nutrient Enrichment and Acidification of Sensitive US Lakes. *BioScience* **2011**, *61* (8), 602–613.
(18) Nanus, L.; McMurray, J. A.; Clow, D. W.; Saros, J. E.; Blett, T.; Gurdak, J. J. Spatial variation of atmospheric nitrogen deposition and critical loads for aquatic ecosystems in the Greater Yellowstone Area. *Environ. Pollut.* **2017**, *223*, 644–656.
(19) Baron, J. S. Hindcasting nitrogen deposition to determine an ecological critical load. *Ecol. Appl.* **2006**, *16* (2), 433–439.
(20) Wolfe, A. P.; Van Gorp, A. C.; Baron, J. S. Recent ecological and biogeochemical changes in alpine lakes of Rocky Mountain National Park (Colorado, USA): a response to anthropogenic nitrogen deposition. *Geobiology* **2003**, *1* (2), 153–168.
(21) Williams, M. W.; Tonnessen, K. A. Critical loads for inorganic nitrogen deposition in the Colorado Front Range, USA. *Ecol. Appl.* **2000**, *10* (6), 1648–1665.
(22) Bassin, S.; Volk, M.; Fuhrer, J. Species Composition of Subalpine Grassland is Sensitive to Nitrogen Deposition, but Not to Ozone, After Seven Years of Treatment. *Ecosystems* **2013**, *16* (6), 1105–1117.
(23) McDonnell, T. C.; Belyazid, S.; Sullivan, T. J.; Sverdrup, H.; Bowman, W. D.; Porter, E. M. Modeled subalpine plant community response to climate change and atmospheric nitrogen deposition in Rocky Mountain National Park, USA. *Environ. Pollut.* **2014**, *187*, 55–64.
(24) Bowman, W. D.; Gartner, J. R.; Holland, K.; Wiedermann, M. Nitrogen Critical Loads For Alpine Vegetation And Terrestrial Ecosystem Response: Are We There Yet? *Ecol. Appl.* **2006**, *16* (3), 1183–1193.
(25) Chapin, F. S.; Walker, B. H.; Hobbs, R. J.; Hooper, D. U.; Lawton, J. H.; Sala, O. E.; Tilman, D. Biotic control over the functioning of ecosystems. *Science* **1997**, *277* (5325), 500–504.
(26) Mast, M. A.; Clow, D. W.; Baron, J. S.; Wetherbee, G. A. Links between N Deposition and Nitrate Export from a High-Elevation Watershed in the Colorado Front Range. *Environ. Sci. Technol.* **2014**, *48* (24), 14258–14265.
(27) Campbell, D. H.; Clow, D. W.; Ingersoll, G. P.; Mast, M. A.; Spahr, N. E.; Turk, J. T. Nitrogen deposition and release in alpine watersheds, Loch Vale, Colorado, USA. *IAHS Publ.-Ser. Proc. Rep.-Intern Assoc Hydrol. Sci.* **1995**, *228*, 243–254.

641 (28) Clow, D. W.; Sueker, J. K. Relations between basin characteristics and stream
642 water chemistry in alpine/subalpine basins in Rocky Mountain National Park, Colorado.
643 *Water Resour. Res.* **2000**, *36* (1), 49–61.
644 (29) Kendall, C.; Campbell, D. H.; Burns, D. A.; Shanley, J. B.; Silva, S. R.; Chang, C. C.
645 Tracing sources of nitrate in snowmelt runoff using the oxygen and nitrogen isotopic
646 compositions of nitrate. *IAHS Publ.-Ser. Proc. Rep.-Intern Assoc Hydrol. Sci.* **1995**, *228*,
647 339–348.
648 (30) OHTE, N.; NAGATA, T.; TAYASU, I.; KOHZU, A.; YOSHIMIZU, C. Nitrogen and
649 oxygen isotope measurements of nitrate to survey the sources and transformation of
650 nitrogen loads in rivers. **2008**.
651 (31) Mayer, B.; Boyer, E. W.; Goodale, C.; Jaworski, N. A.; Van Breemen, N.; Howarth, R.
652 W.; Seitzinger, S.; Billen, G.; Lajtha, K.; Nadelhoffer, K.; et al. Sources of nitrate in rivers
653 draining sixteen watersheds in the northeastern US: Isotopic constraints.
654 *Biogeochemistry* **2002**, *57* (1), 171–197.
655 (32) Michalski, G.; Meixner, T.; Fenn, M.; Hernandez, L.; Sirulnik, A.; Allen, E.;
656 Thiemens, M. Tracing Atmospheric Nitrate Deposition in a Complex Semiarid Ecosystem
657 Using Δ17O. *Environ. Sci. Technol.* **2004**, *38* (7), 2175–2181.
658 (33) Liu, T.; Wang, F.; Michalski, G.; Xia, X.; Liu, S. Using ^{15} N, ^{17} O, and ^{18} O To
659 Determine Nitrate Sources in the Yellow River, China. *Environ. Sci. Technol.* **2013**, *47*
660 (23), 13412–13421.
661 (34) Rose, L. A.; Elliott, E. M.; Adams, M. B. Triple Nitrate Isotopes Indicate Differing
662 Nitrate Source Contributions to Streams Across a Nitrogen Saturation Gradient.
663 *Ecosystems* **2015**, *18* (7), 1209–1223.
664 (35) Tsunogai, U.; Miyauchi, T.; Ohyama, T.; Komatsu, D. D.; Nakagawa, F.; Obata, Y.;
665 Sato, K.; Ohizumi, T. Accurate and precise quantification of atmospheric nitrate in
666 streams draining land of various uses by using triple oxygen isotopes as tracers.
667 *Biogeosciences* **2016**, *13* (11), 3441–3459.
668 (36) Legay, N.; Grassein, F.; Robson, T. M.; Personeni, E.; Bataillé, M.-P.; Lavorel, S.;
669 Clément, J.-C. Comparison of inorganic nitrogen uptake dynamics following snowmelt
670 and at peak biomass in subalpine grasslands. *Biogeosciences* **2013**, *10* (11), 7631–7645.
671 (37) Clement, J. C.; Robson, T. M.; Guillemin, R.; Saccone, P.; Lochet, J.; Aubert, S.;
672 Lavorel, S. The effects of snow-N deposition and snowmelt dynamics on soil-N cycling in
673 marginal terraced grasslands in the French Alps. *Biogeochemistry* **2012**, *108* (1–3), 297–
674 315.
675 (38) Jaffrezo, J.-L.; Aymoz, G.; Cozic, J. Size distribution of EC and OC in the aerosol of
676 Alpine valleys during summer and winter. *Atmospheric Chem. Phys.* **2005**, *5* (11), 2915–
677 2925.
678 (39) Williams, M. W.; Melack, J. M. Solute chemistry of snowmelt and runoff in an
679 Alpine Basin, Sierra Nevada. *Water Resour. Res.* **1991**, *27* (7), 1575–1588.
680 (40) Erbland, J. Contraintes isotopiques sur l'interprétation de l'enregistrement en
681 nitrate dans la carotte de glace de Vostok, Université de Grenoble, 2011.
682 (41) Templer, P. H.; Weathers, K. C. Use of mixed ion exchange resin and the denitrifier
683 method to determine isotopic values of nitrate in atmospheric deposition and canopy
684 throughfall. *Atmos. Environ.* **2011**, *45* (11), 2017–2020.
685 (42) Wood, E. D.; Armstrong, F. A. J.; Richards, F. A. Determination of nitrate in sea
686 water by cadmium-copper reduction to nitrite. *J. Mar. Biol. Assoc. U. K.* **1967**, *47* (1), 23.
687 (43) Casciotti, K. L.; Sigman, D. M.; Hastings, M. G.; Böhlke, J. K.; Hilkert, A.
688 Measurement of the Oxygen Isotopic Composition of Nitrate in Seawater and Freshwater
689 Using the Denitrifier Method. *Anal. Chem.* **2002**, *74* (19), 4905–4912.

690 (44) Kaiser, J.; Hastings, M. G.; Houlton, B. Z.; Röckmann, T.; Sigman, D. M. Triple
691 Oxygen Isotope Analysis of Nitrate Using the Denitrifier Method and Thermal
692 Decomposition of N_2O. *Anal. Chem.* **2007**, *79* (2), 599–607.
693 (45) Morin, S.; Savarino, J.; Frey, M. M.; Yan, N.; Bekki, S.; Bottenheim, J. W.; Martins, J.
694 M. F. Tracing the Origin and Fate of NOx in the Arctic Atmosphere Using Stable Isotopes
695 in Nitrate. *Science* **2008**, *322* (5902), 730–732.
696 (46) Morin, S.; Savarino, J.; Frey, M. M.; Domine, F.; Jacobi, H.-W.; Kaleschke, L.;
697 Martins, J. M. F. Comprehensive isotopic composition of atmospheric nitrate in the
698 Atlantic Ocean boundary layer from 65°S to 79°N. *J. Geophys. Res.* **2009**, *114* (D5).
699 (47) Thiemens, M. H. History and applications of mass-independent isotope effects.
700 *Annu Rev Earth Planet Sci* **2006**, *34*, 217–262.
701 (48) Kaiser, J. Technical note: Consistent calculation of aquatic gross production from
702 oxygen triple isotope measurements. *Biogeosciences* **2011**, *8* (7), 1793–1811.
703 (49) Savarino, J.; Kaiser, J.; Morin, S.; Sigman, D. M.; Thiemens, M. H. Nitrogen and
704 oxygen isotopic constraints on the origin of atmospheric nitrate in coastal Antarctica.
705 *Atmospheric Chem. Phys.* **2007**, *7* (8), 1925–1945.
706 (50) Michalski, G.; Kolanowski, M.; Riha, K. M. Oxygen and nitrogen isotopic
707 composition of nitrate in commercial fertilizers, nitric acid, and reagent salts. *Isotopes
708 Environ. Health Stud.* **2015**, *51* (3), 382–391.
709 (51) Kendall, C.; Elliott, E. M.; Wankel, S. D. Tracing anthropogenic inputs of nitrogen
710 to ecosystems. *Stable Isot. Ecol. Environ. Sci.* **2007**, *2*, 375–449.
711 (52) Granger, J.; Sigman, D. M.; Rohde, M. M.; Maldonado, M. T.; Tortell, P. D. N and O
712 isotope effects during nitrate assimilation by unicellular prokaryotic and eukaryotic
713 plankton cultures. *Geochim. Cosmochim. Acta* **2010**, *74* (3), 1030–1040.
714 (53) Granger, J.; Wankel, S. D. Isotopic overprinting of nitrification on denitrification as
715 a ubiquitous and unifying feature of environmental nitrogen cycling. *Proc. Natl. Acad. Sci.
716* **2016**, *113* (42), E6391–E6400.
717 (54) Savarino, J.; Morin, S.; Erbland, J.; Grannec, F.; Patey, M. D.; Vicars, W.; Alexander,
718 B.; Achterberg, E. P. Isotopic composition of atmospheric nitrate in a tropical marine
719 boundary layer. *Proc. Natl. Acad. Sci.* **2013**, *110* (44), 17668–17673.
720 (55) Elliott, E. M.; Kendall, C.; Boyer, E. W.; Burns, D. A.; Lear, G. G.; Golden, H. E.;
721 Harlin, K.; Bytnerowicz, A.; Butler, T. J.; Glatz, R. Dual nitrate isotopes in dry deposition:
722 Utility for partitioning NO_x source contributions to landscape nitrogen deposition. *J.
723 Geophys. Res.* **2009**, *114* (G4).
724 (56) Campbell, D. H.; Kendall, C.; Chang, C. C. Y.; Silva, S. R.; Tonnessen, K. A. Pathways
725 for nitrate release from an alpine watershed: Determination using $\delta^{15}N$ and $\delta^{18}O$:
726 ALPINE WATERSHED NITRATE $\delta^{15}N$ AND $\delta^{18}O$. *Water Resour. Res.* **2002**, *38* (5), 10-1-
727 10–19.
728 (57) Burns, D. A.; Kendall, C. Analysis of δ15N and δ18O to differentiate NO3− sources
729 in runoff at two watersheds in the Catskill Mountains of New York. *Water Resour. Res.
730* **2002**, *38* (5), 9–1.
731 (58) Rose, L. A.; Sebestyen, S. D.; Elliott, E. M.; Koba, K. Drivers of atmospheric nitrate
732 processing and export in forested catchments. *Water Resour. Res.* **2015**, *51* (2), 1333–
733 1352.
734 (59) Hastings, M. G. Seasonal variations in N and O isotopes of nitrate in snow at
735 Summit, Greenland: Implications for the study of nitrate in snow and ice cores. *J.
736 Geophys. Res.* **2004**, *109* (D20).
737 (60) Williams, M. W.; Seibold, C.; Chowanski, K. Storage and release of solutes from a
738 subalpine seasonal snowpack: soil and stream water response, Niwot Ridge, Colorado.

739 *Biogeochemistry* **2009**, *95* (1), 77–94.
740 (61) Campbell, J. L.; Mitchell, M. J.; Mayer, B.; Groffman, P. M.; Christenson, L. M.
741 Mobility of Nitrogen-15-Labeled Nitrate and Sulfur-34-Labeled Sulfate during Snowmelt.
742 *Soil Sci. Soc. Am. J.* **2007**, *71* (6), 1934.
743 (62) Brooks, P. D.; Williams, M. W. Snowpack controls on nitrogen cycling and export
744 in seasonally snow-covered catchments. *Hydrol. Process.* **1999**, *13* (14), 2177–2190.
745 (63) Nanus, L.; Williams, M. W.; Campbell, D. H.; Elliott, E. M.; Kendall, C. Evaluating
746 Regional Patterns in Nitrate Sources to Watersheds in National Parks of the Rocky
747 Mountains using Nitrate Isotopes. *Environ. Sci. Technol.* **2008**, *42* (17), 6487–6493.
748 (64) Darrouzet-Nardi, A.; Erbland, J.; Bowman, W. D.; Savarino, J.; Williams, M. W.
749 Landscape-level nitrogen import and export in an ecosystem with complex terrain,
750 Colorado Front Range. *Biogeochemistry* **2012**, *109* (1–3), 271–285.
751 (65) Snider, D. M.; Spoelstra, J.; Schiff, S. L.; Venkiteswaran, J. J. Stable Oxygen Isotope
752 Ratios of Nitrate Produced from Nitrification: 18O-Labeled Water Incubations of
753 Agricultural and Temperate Forest Soils. *Environ. Sci. Technol.* **2010**, *44* (14), 5358–
754 5364.
755 (66) Xue, D.; Botte, J.; De Baets, B.; Accoe, F.; Nestler, A.; Taylor, P.; Van Cleemput, O.;
756 Berglund, M.; Boeckx, P. Present limitations and future prospects of stable isotope
757 methods for nitrate source identification in surface- and groundwater. *Water Res.* **2009**,
758 *43* (5), 1159–1170.
759 (67) Mara, P.; Mihalopoulos, N.; Gogou, A.; Daehnke, K.; Schlarbaum, T.; Emeis, K.-C.;
760 Krom, M. Isotopic composition of nitrate in wet and dry atmospheric deposition on Crete
761 in the eastern Mediterranean Sea: ISOTOPIC COMPOSITION OF NITRATE IN
762 DEPOSITION. *Glob. Biogeochem. Cycles* **2009**, *23* (4), n/a-n/a.
763 (68) Guha, T.; Lin, C. T.; Bhattacharya, S. K.; Mahajan, A. S.; Ou-Yang, C.-F.; Lan, Y.-P.;
764 Hsu, S. C.; Liang, M.-C. Isotopic ratios of nitrate in aerosol samples from Mt. Lulin, a high-
765 altitude station in Central Taiwan. *Atmos. Environ.* **2017**, *154*, 53–69.
766 (69) Jusselme, M.-D.; Saccone, P.; Zinger, L.; Faure, M.; Le Roux, X.; Guillaumaud, N.;
767 Bernard, L.; Clement, J.-C.; Poly, F. Variations in snow depth modify N-related soil
768 microbial abundances and functioning during winter in subalpine grassland. *Soil Biol.*
769 *Biochem.* **2016**, *92*, 27–37.
770 (70) Hiltbrunner, E.; Schwikowski, M.; Körner, C. Inorganic nitrogen storage in alpine
771 snow pack in the Central Alps (Switzerland). *Atmos. Environ.* **2005**, *39* (12), 2249–2259.
772 (71) Schmidt, S. K.; Lipson, D. A. Microbial growth under the snow: implications for
773 nutrient and allelochemical availability in temperate soils. *Plant Soil* **2004**, *259* (1), 1–7.
774 (72) Williams, M. W.; Brooks, P. D.; Mosier, A.; Tonnessen, K. A. Mineral nitrogen
775 transformations in and under seasonal snow in a high-elevation catchment in the Rocky
776 Mountains, United States. *Water Resour. Res.* **1996**, *32* (10), 3161–3171.
777 (73) Saccone, P.; Morin, S.; Baptist, F.; Bonneville, J.-M.; Colace, M.-P.; Domine, F.;
778 Faure, M.; Geremia, R.; Lochet, J.; Poly, F.; et al. The effects of snowpack properties and
779 plant strategies on litter decomposition during winter in subalpine meadows. *Plant Soil*
780 **2013**, *363* (1–2), 215–229.
781 (74) Liu, F.; Williams, M. W.; Caine, N. Source waters and flow paths in an alpine
782 catchment, Colorado Front Range, United States: SOURCE WATERS AND FLOW PATHS
783 IN ALPINE CATCHMENTS. *Water Resour. Res.* **2004**, *40* (9).
784 (75) Cowie, R. M.; Knowles, J. F.; Dailey, K. R.; Williams, M. W.; Mills, T. J.; Molotch, N. P.
785 Sources of streamflow along a headwater catchment elevational gradient. *J. Hydrol.*
786 **2017**, *549*, 163–178.
787 (76) Bodin, X.; Thibert, E.; Fabre, D.; Ribolini, A.; Schoeneich, P.; Francou, B.; Reynaud,

L.; Fort, M. Two decades of responses (1986–2006) to climate by the Laurichard rock glacier, French Alps. *Permafr. Periglac. Process.* **2009**, *20* (4), 331–344.
(77) Williams, M. W.; Knauf, M.; Cory, R.; Caine, N.; Liu, F. Nitrate content and potential microbial signature of rock glacier outflow, Colorado Front Range. *Earth Surf. Process. Landf.* **2007**, *32* (7), 1032–1047.
(78) Saros, J. E.; Rose, K. C.; Clow, D. W.; Stephens, V. C.; Nurse, A. B.; Arnett, H. A.; Stone, J. R.; Williamson, C. E.; Wolfe, A. P. Melting Alpine Glaciers Enrich High-Elevation Lakes with Reactive Nitrogen. *Environ. Sci. Technol.* **2010**, *44* (13), 4891–4896.
(79) Slemmons, K. E. H.; Saros, J. E.; Simon, K. The influence of glacial meltwater on alpine aquatic ecosystems: a review. *Environ. Sci. Process. Impacts* **2013**, *15* (10), 1794.
(80) Williams, J. J.; Nurse, A.; Saros, J. E.; Riedel, J.; Beutel, M. Effects of glaciers on nutrient concentrations and phytoplankton in lakes within the Northern Cascades Mountains (USA). *Biogeochemistry* **2016**, *131* (3), 373–385.
(81) Hood, E.; Scott, D. Riverine organic matter and nutrients in southeast Alaska affected by glacial coverage. *Nat. Geosci.* **2008**, *1* (9), 583–587.
(82) Barnes, R. T.; Williams, M. W.; Parman, J. N.; Hill, K.; Caine, N. Thawing glacial and permafrost features contribute to nitrogen export from Green Lakes Valley, Colorado Front Range, USA. *Biogeochemistry* **2014**, *117* (2–3), 413–430.
(83) Louiseize, N. L.; Lafrenière, M. J.; Hastings, M. G. Stable isotopic evidence of enhanced export of microbially derived $${\text{NO}}_{3}^{ - }$$ NO 3 - following active layer slope disturbance in the Canadian High Arctic. *Biogeochemistry* **2014**, *121* (3), 565–580.
(84) Balestrini, R.; Arese, C.; Freppaz, M.; Buffagni, A. Catchment features controlling nitrogen dynamics in running waters above the tree line (central Italian Alps). *Hydrol. Earth Syst. Sci.* **2013**, *17* (3), 989–1001.
(85) Hall Jr, R. O.; Baker, M. A.; Arp, C. D.; Koch, B. J. Hydrologic control of nitrogenremoval, storage and export in a mountain stream. *Limnol. Oceanogr.* **2009**, *54*, 2128.
(86) Lovett, G. M.; Goodale, C. L. A New Conceptual Model of Nitrogen Saturation Based on Experimental Nitrogen Addition to an Oak Forest. *Ecosystems* **2011**, *14* (4), 615–631.
(87) Boutin, M.; Lamaze, T.; Couvidat, F.; Pornon, A. Subalpine Pyrenees received higher nitrogen deposition than predicted by EMEP and CHIMERE chemistry-transport models. *Sci. Rep.* **2015**, *5* (1).
(88) Hundey, E. J.; Russell, S. D.; Longstaffe, F. J.; Moser, K. A. Agriculture causes nitrate fertilization of remote alpine lakes. *Nat. Commun.* **2016**, *7*, 10571.
(89) Tsunogai, U.; Daita, S.; Komatsu, D. D.; Nakagawa, F.; Tanaka, A. Quantifying nitrate dynamics in an oligotrophic lake using Δ¹⁷O. *Biogeosciences* **2011**, *8* (3), 687–702.
(90) Hobbs, W. O.; Lafrancois, B. M.; Stottlemyer, R.; Toczydlowski, D.; Engstrom, D. R.; Edlund, M. B.; Almendinger, J. E.; Strock, K. E.; VanderMeulen, D.; Elias, J. E.; et al. Nitrogen deposition to lakes in national parks of the western Great Lakes region: Isotopic signatures, watershed retention, and algal shifts: NITROGEN DEPOSITION TO NORTHERN LAKES. *Glob. Biogeochem. Cycles* **2016**, *30* (3), 514–533.
(91) Spaulding, S. A.; Otu, M. K.; Wolfe, A. P.; Baron, J. S. Paleolimnological Records of Nitrogen Deposition in Shallow, High-Elevation Lakes of Grand Teton National Park, Wyoming, U.S.A. *Arct. Antarct. Alp. Res.* **2015**, *47* (4), 703–717.
(92) Elser, J. J.; Andersen, T.; Baron, J. S.; Bergström, A.-K.; Jansson, M.; Kyle, M.; Nydick, K. R.; Steger, L.; Hessen, D. O. Shifts in lake N:P stoichiometry and nutrient limitation driven by atmospheric nitrogen deposition. *Science* **2009**, *326* (5954), 835–837.

837 (93) Bilbrough, C. J.; Welker, J. M.; Bowman, W. D. Early Spring Nitrogen Uptake by
838 Snow-Covered Plants: A Comparison of Arctic and Alpine Plant Function under the
839 Snowpack. *Arct. Antarct. Alp. Res.* **2000**, *32* (4), 404.

840 **List of Figures**

841

842 **Table 1** Mean volume-weighted concentration and concentration-weighted isotopic
843 values for NO_3^- in snow pits (SP) and aerosols at the Lautaret Pass. Snow pits mean
844 values are always calculated over the entire depth of the snow pack. Dates for SP
845 are given in a dd/mm/yy format. SD is the standard deviation.

846

847 **Figure 1** Seasonal variations of a) log([NO_3^-] in $\mu g.L^{-1}$) (for an easier comparison of
848 streams [NO_3^-]); b) $\Delta^{17}O$ (‰) and corresponding f_{atm} (%, the relative amount of
849 atmospheric nitrate in streams); c) $\delta^{18}O$ (‰) and d) $\delta^{15}N$ (‰) of NO_3^- in streams
850 Red, blue and green colors stand for Tufiere, Laurichard and Romanche,
851 respectively. Highlighted in yellow is a two-days rainstorm that occurred mid-June.
852 The grey frames highlight the dormant season while the green one highlights the
853 growing season. Transitions between both seasons are snowmelt period in spring,
854 and plant senescence in autumn.

855

Figure 2 Correlation between nitrate $\Delta^{17}O$ (‰) and a), b), c) log([NO_3^-]); d), e), f) $\delta^{18}O$ (‰); g), h), i) $\delta^{15}N$ (‰).

Red, blue and green colors stand for Tufiere, Laurichard and Romanche, respectively. Outliers (surrounded by stars) were not considered in the linear regression model, as we assume they result from biological processes (*e.g.*, denitrification) and would blur determination of NO_3^- sources.

Figure 3 Dual isotopes plot ($\Delta^{17}O$ *vs.* $\delta^{15}N$) illustrating the mixing between three sources of NO_3^- in our study sites. The plain triangles feature the mixing range between snow $NO_3^-_{atm}$ and NO_3^- from nitrified $NH_4^+_{atm}$ in grey, NO_3^- from nitrified $NH_4^+_{bio}$ in turquoise and NO_3^- from manure or sewage in beige. The dashed triangles of similar colors (*i.e.*, grey-turquoise and turquoise-beige) illustrate the overlapping of sources $\delta^{15}N\text{-}NO_3^-$ values. The dashed purple triangle illustrates the mixing range between $NO_3^-_{atm}$ and NO_3^- from nitrified $NH_4^+_{bio}$ if summer deposition was the atmospheric end-member.

When $\Delta^{17}O\text{-}NO_3^-$ values are high, $\delta^{15}N\text{-}NO_3^-$ is characteristic of nitrified $NH_4^+_{atm}$, delineating the coupled contribution of atmospheric N deposition *via* direct inputs ($NO_3^-_{atm}$) and indirect inputs (nitrified $NH_4^+_{atm}$). Decreased contribution of atmospheric N sources (low $\Delta^{17}O\text{-}NO_3^-$ values) results in a higher proportion of $NO_3^-_{bio}$.

	Snow depth (cm)	$\delta^{15}N$ (‰)	$\delta^{18}O$ (‰)	$\Delta^{17}O$ (‰)	$[NO_3^-]$ ($mg.L^{-1}$)
		Mean (SD)	Mean (SD)	Mean (SD)	Mean (SD)
SP 09/12/14	66	-5.5 (2.7)	77.0 (5.0)	29.8 (1.9)	0.1 (0.4)
SP 13/01/15	64	-3.6 (1.7)	76.6 (7.2)	28.6 (2.5)	0.1 (0.9)
SP 19/02/15	139	-2.4 (1.2)	77.7 (4.5)	29.3 (1.2)	1.2 (1.3)
SP 19/03/15	142	-2.3 (1.6)	76.3 (4.6)	28.5 (1.3)	0.9 (1.0)
SP 09/04/15	104	-4.1 (1.1)	77.2 (6.8)	30.1 (1.0)	0.6 (0.6)
Aerosols (summer)	-	-6.5 (3.6)	62.9 (6.5)	23.1 (2.4)	0.1 (0.1) $mg.m^{-3}$
Aerosols (winter)	-	-1.0 (1.7)	74.7 (4.4)	28.9 (1.0)	0.1 (0.2) $mg.m^{-3}$

Table 1

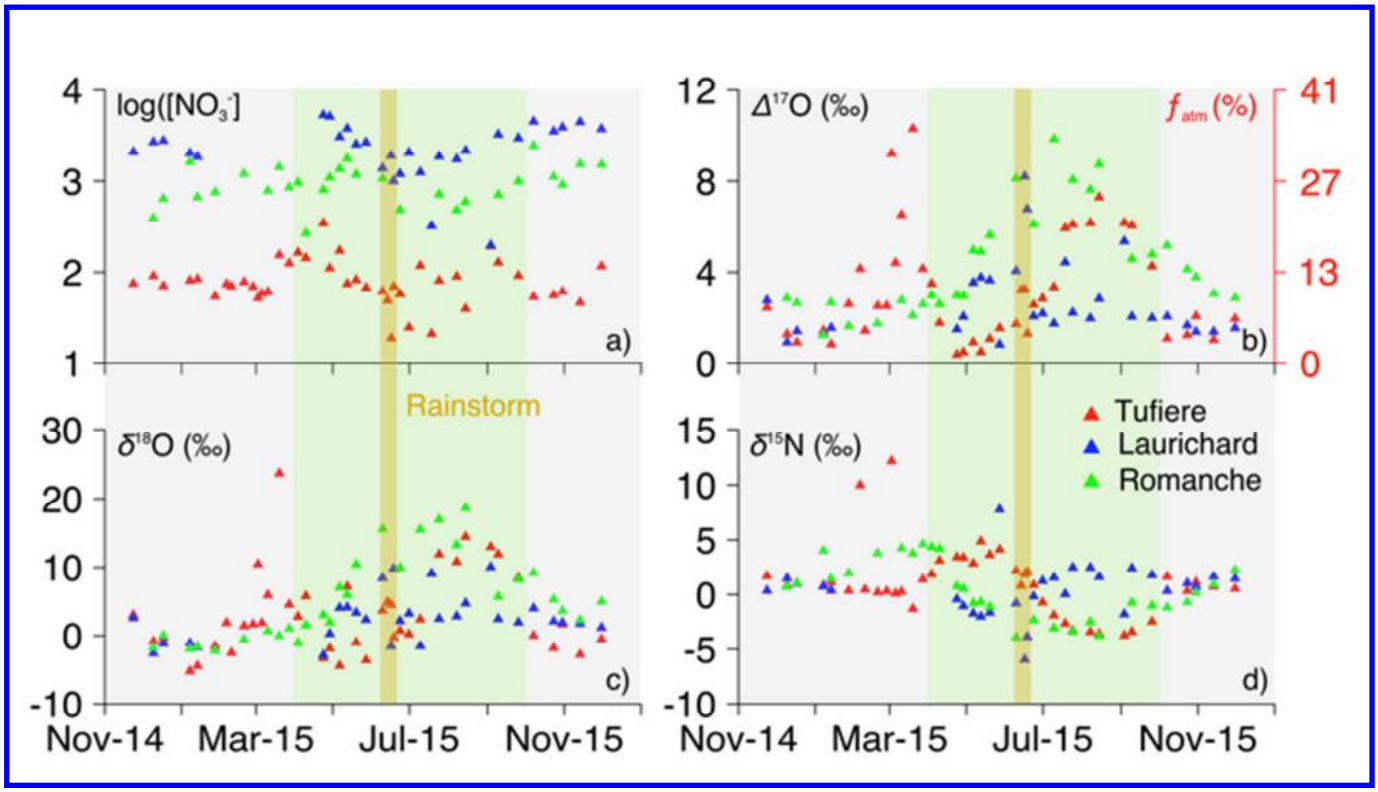

Figure 1

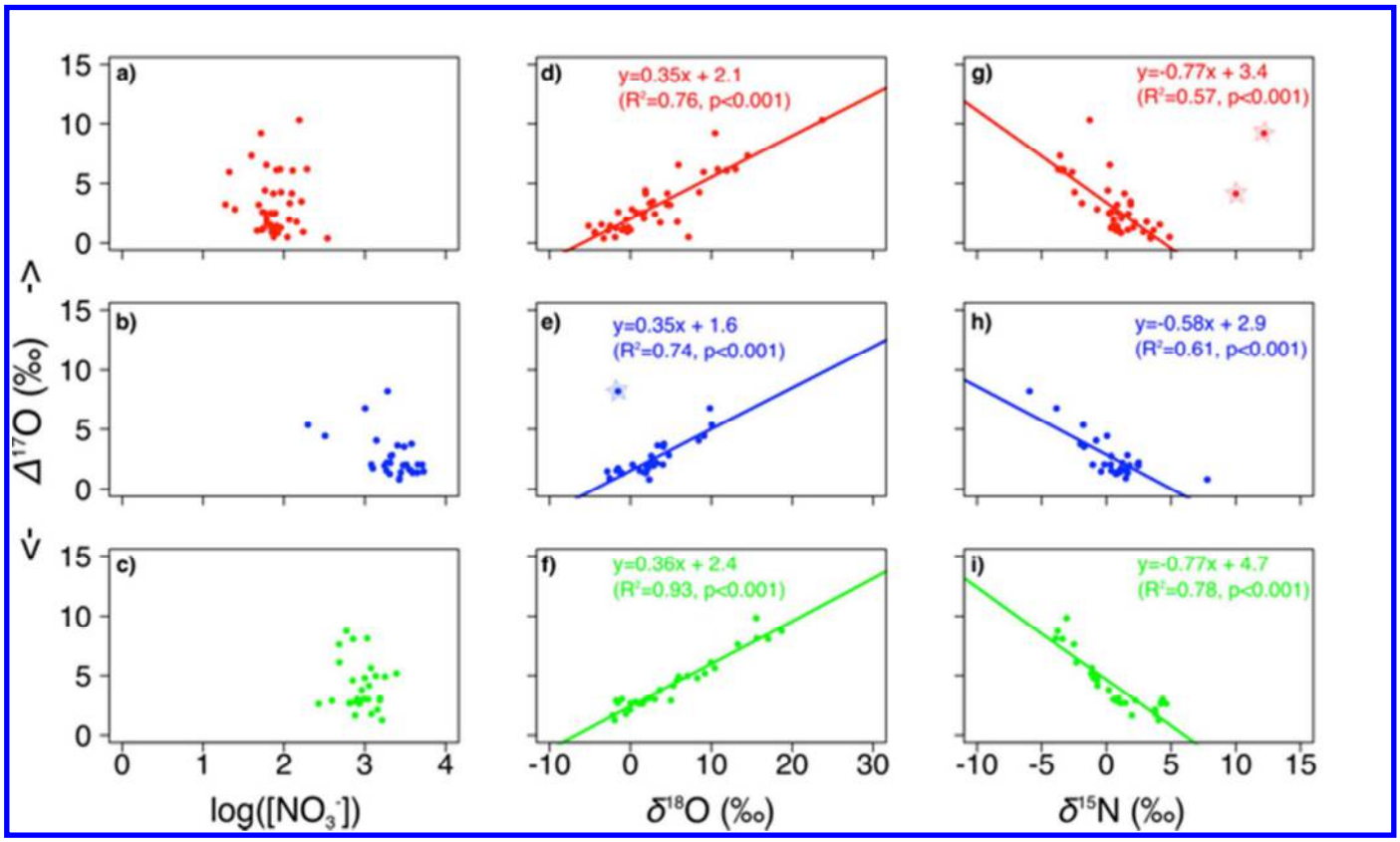

Figure 2

ACS Paragon Plus Environment

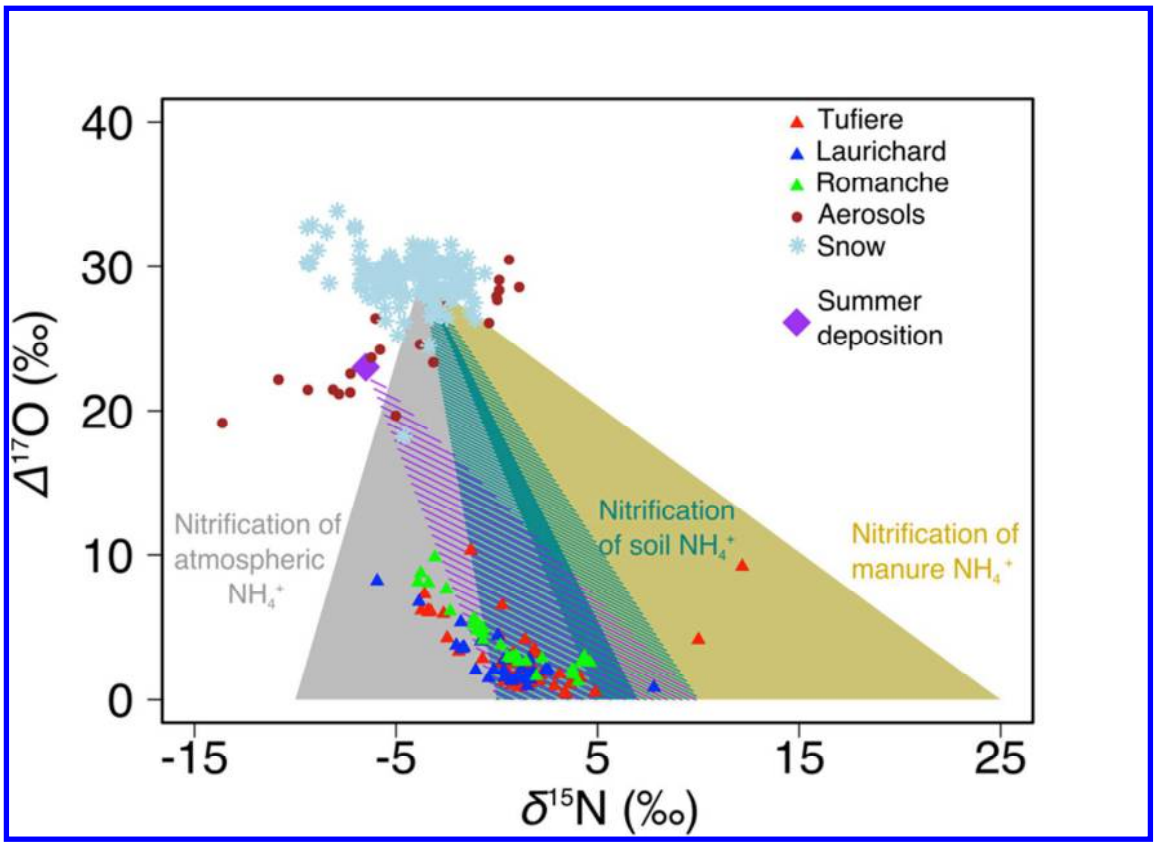

Figure 3